Broadband Beam Smoothing on OMEGA with Two-Dimensional Smoothing by Spectral Dispersion

High laser-irradiation uniformity is an important requirement for successful implosions of inertial confinement fusion (ICF) targets,[1] particularly for the direct-drive OMEGA laser system that directly illuminates ICF targets. Direct-drive laser irradiation that is not perfectly uniform imprints on the target surface and perturbs the spherical symmetry. This seeds the Rayleigh–Taylor hydrodynamic instability during the target acceleration phase and can severely degrade target performance. Target imprinting is determined when the critical surface decouples from the ablation surface. The critical surface corresponds to the highest density reached by the plasma, where the laser frequency equals the plasma frequency. The ablation surface corresponds roughly to the surface separating the inward-flowing (imploding) plasma and the outward-flowing "exhaust." Direct-drive smoothing techniques must minimize the level of irradiation nonuniformity on a time scale comparable to or shorter than this imprinting phase. Initial target experiments indicate that this imprinting phase lasts for several hundred picoseconds on OMEGA and depends on the spatial wavelength of the most important perturbations.

Direct-drive laser irradiation uniformity for different ranges of spatial frequencies is achieved on OMEGA by a number of techniques.[1] The number of beams, as well as power and energy balance among beams, predominantly affects irradiation nonuniformity at low spatial frequencies, while higher spatial frequencies are determined by the individual beam uniformity achievable with smoothing by spectral dispersion (SSD).

The technique of SSD significantly reduces irradiation nonuniformity by rapidly shifting the laser speckle pattern generated on the target by distributed phase plates (DPP's).[2] A high-frequency electro-optic phase modulator produces a time-varying wavelength modulation that is angularly dispersed by a diffraction grating. Significant smoothing is achieved on a time scale approximately equal to the inverse bandwidth impressed by the phase modulator. Two-dimensional SSD (2-D SSD) extends the smoothing benefits of SSD by combining the deflections of the laser speckle pattern on target in two orthogonal directions. Two separate stages of bulk electro-optic phase modulators and gratings are employed that generate and disperse bandwidth in two orthogonal directions.

Broadband Two-Dimensional SSD Generation

The principal relationships governing irradiation uniformity with SSD are illustrated in Fig. 80.6(a), which plots the rms irradiation nonuniformity for all spatial frequencies (for modes with $\ell \leq 500$) on target for several different SSD configurations versus integrating time. The initial smoothing rate is directly proportional to the SSD bandwidth since the coherence time for the speckle pattern produced by the DPP is inversely related to the effective bandwidth in any time slice of the pulse. The asymptotic nonuniformity is inversely related to the square root of the number of independent speckle patterns on the target. For an SSD system employing critical dispersion, this corresponds to the number of FM sidebands imposed on the beam by the phase modulator.

Incorporating a higher-frequency phase modulator in the 2-D SSD system offers two different approaches to improving irradiation uniformity on OMEGA: increasing the total SSD bandwidth or producing multiple SSD color cycles.

1. Large SSD bandwidths can be generated for a given number of critically dispersed FM sidebands and propagated through the laser system since less grating dispersion is required to achieve a single color cycle. Increased SSD bandwidths smooth laser irradiation faster. An asymmetric 2-D SSD configuration on OMEGA using phase modulators operating at 3.3 and 10.4 GHz can produce infrared bandwidths of 1.5×11 Å at nominally 1×1 color cycles, respectively. This infrared bandwidth corresponds to a UV bandwidth of approximately 1 THz.

2. Multiple SSD color cycles can be produced with a higher modulation frequency using the current grating design without exceeding the beam divergence limit imposed by the laser system pinholes. Increasing the number of color cycles accelerates the smoothing at the mid-range spatial frequencies (ℓ = 50–200) that pose the greatest threat of

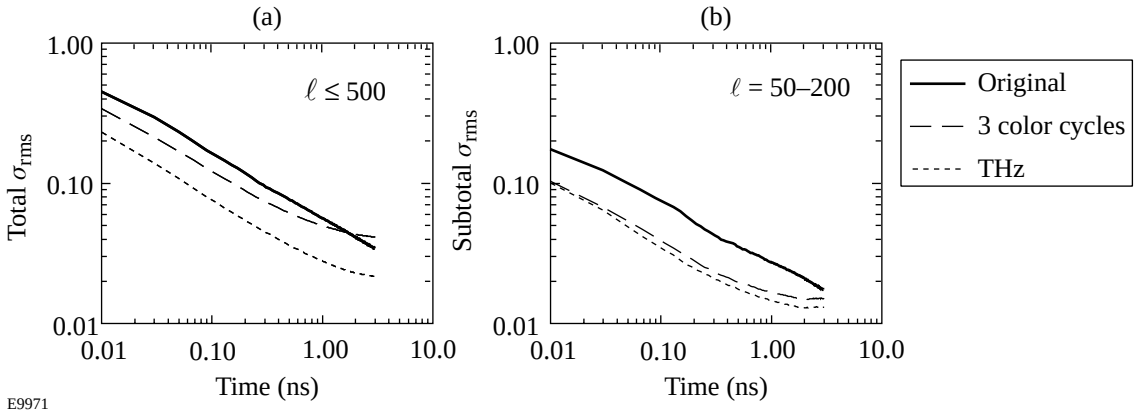

Figure 80.6
The intial rate of SSD smoothing is governed by the total bandwidth, while the asymptotic nonuniformity is related to the total number of independent speckle patterns on target. If at least one SSD color cycle is present, this corresponds to the number of FM sidebands produced by the phase modulators. (a) Plotting total nonuniformity ($\ell \leq 500$) versus averaging time shows that comparable smoothing levels should be achieved approximately four times sooner with the 1-THz SSD (1.5 × 11 Å, 1 × 1 color cycles) system than the original 2-D SSD (1.25 × 1.75 Å, 1 × 1 color cycles) system implemented on OMEGA, while the three-color-cycle 2-D SSD (1.5 × 3 Å, 1 × 3 color cycles) system actually achieves worse asymptotic levels since fewer independent speckles modes are produced. (b) Smoothing performance for the spatial frequencies associated with ℓ-modes in the range between 50 and 200 shows different behavior. The three-color-cycle SSD system performance during the first stage of smoothing is comparable to the 1-THz SSD system since the multiple color cycles preferentially smooth these spatial frequencies.

seeding hydrodynamic instabilities in direct-drive implosions. The current OMEGA FCC configuration can efficiently convert infrared bandwidths of 1.5 × 3.0 Å from modulators operating at 3.3 and 10.4 GHz to generate 1 × 3 color cycles, respectively.

The single-beam smoothing performance for several 2-D SSD implementations on OMEGA is compared in Fig. 80.6. Total rms nonuniformity is plotted versus integration time in Fig. 80.6(a). The original 2-D SSD implementation on OMEGA delivered approximately 0.2 THz of total SSD bandwidth in the ultraviolet (1.25 × 1.75 Å IR, 1 × 1 color cycles). Asymptotic nonuniformity levels of better than 2% are achieved after approximately 250 ps when multiple-beam overlap is included. In comparison, the 1-THz system (1.5 × 11 Å, 1 × 1 color cycles) planned for installation in November 1999 achieves improved asymptotic uniformity since it produces a larger number of independent speckle patterns and larger beam deflections. Furthermore, the integration time required to achieve 2% nonuniformity is reduced to about 70 ps.

The total smoothing performance of the three-color-cycle 2-D SSD system recently installed on OMEGA (1.5 × 3.0 Å, 1 × 3 color cycles) is also shown in Fig. 80.6(a). Poorer asymptotic performance is expected than for either of the other two systems since fewer independent speckle patterns are produced. Figure 80.6(b) presents the rms nonuniformity for the mid-range spatial frequencies versus integration time for the same 2-D SSD systems shown in Fig. 80.6(a). For these spatial frequencies, it can be seen that the smoothing performance of the three-color-cycle system is comparable to the 1-THz system. Direct comparisons of the target performance with both of these improved 2-D SSD systems will be performed once the 1-THz system is implemented.

For OMEGA, it is advantageous to implement the larger bandwidth and beam divergence in the second direction of the 2-D SSD setup since the bandwidth from the second modulator is not dispersed until after the most-limiting spatial-filter pinhole located in the large-aperture ring amplifier (LARA)[3] in the driver line. This constraint results from spatial-filtering requirements associated with the serrated aperture apodizer used to set the OMEGA beam profile. A slotted LARA spatial-filter pinhole with its long axis aligned along the direction of dispersed bandwidth is employed to maximize spatial filtering of the beam.

Larger spatial-filter pinholes are another important requirement for propagating broadband 2-D SSD on OMEGA. Pinhole sizes for the spatial filters in each of the six stages of OMEGA were originally chosen such that computed instantaneous intensities on the edge of any pinhole did not exceed 100 GW/cm^2[4] for a non-SSD, 1-ns FWHM Gaussian pulse. To perform this computation, a complete diffraction and non-

linear propagation model of the system was constructed. Amplitude noise, using the data of Stowers and Patton,[5,6] was applied to optical surfaces and the resulting pinhole irradiance calculated. For pinholes early in the system where spatial noise and its nonlinear growth were not an issue, the pinhole sizes were set no lower than approximately 13 times diffraction-limited in order to facilitate fabrication and alignment. Later optical time-domain reflectometry (OTDR) measurements on OMEGA indicated that in the beamline stages, the pinhole sizes were close to optimum for non-SSD high-energy shots. These same pinholes were operated with 1.25×1.75-Å bandwidth SSD with no deleterious effect or resultant amplitude modulation. Spatial noise measurements were also performed on OMEGA using a high-dynamic-range, far-field diagnostic, as shown in Fig. 80.7. The nonlinear growth of this noise was analyzed to establish the largest acceptable pinholes.

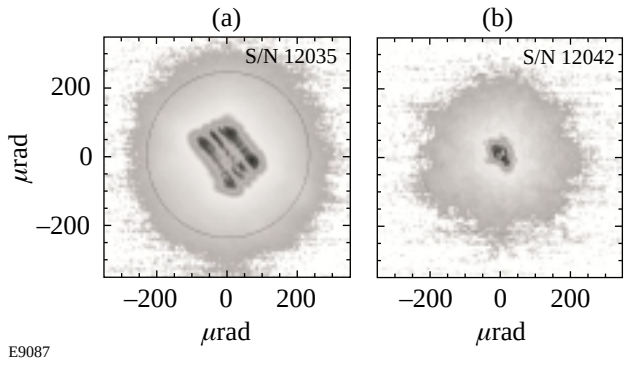

Figure 80.7
OMEGA spatial noise measurements and growth analysis set how much pinholes could be enlarged to accommodate broadband 2-D SSD.

For the current 1.5×3.0-Å SSD bandwidths, the pinholes were increased in diameter by the increase in the major dimension of the far-field spot (~50%). Since increased pinhole size increased the risk of system damage due to ripple growth[7] and Narcissus[8] (pencil beam) spots, a single beamline (40) of OMEGA was operated with these larger pinholes for a full year prior to their installation in the remainder of the system. No damage was observed in any of the optics in that beamline, which was exercised over the full range of OMEGA output energy and pulse shapes.

The 2-D SSD architecture implementing double-pass phase modulators and gratings shown in Fig. 80.8 was chosen for several reasons. Double-pass operation of a phase modulator increases its effective modulation efficiency, provided proper phase matching of the second pass is maintained. As a result, significantly lower microwave powers are required to achieve a given bandwidth while reducing the risk of air breakdown from the microwave fields in the microwave modulator resonators. Multiple-pass modulator operation can further increase the modulation efficiency but at the expense of increased system complexity.

Including a double-pass grating in the first SSD dimension also significantly reduces the space envelope required. Combining the first dimension predelay (G1) and dispersion (G2) functions into a single grating requires a far-field retroreflection to accomplish an image inversion; otherwise, the second pass through the grating would produce additional pulse distortion.

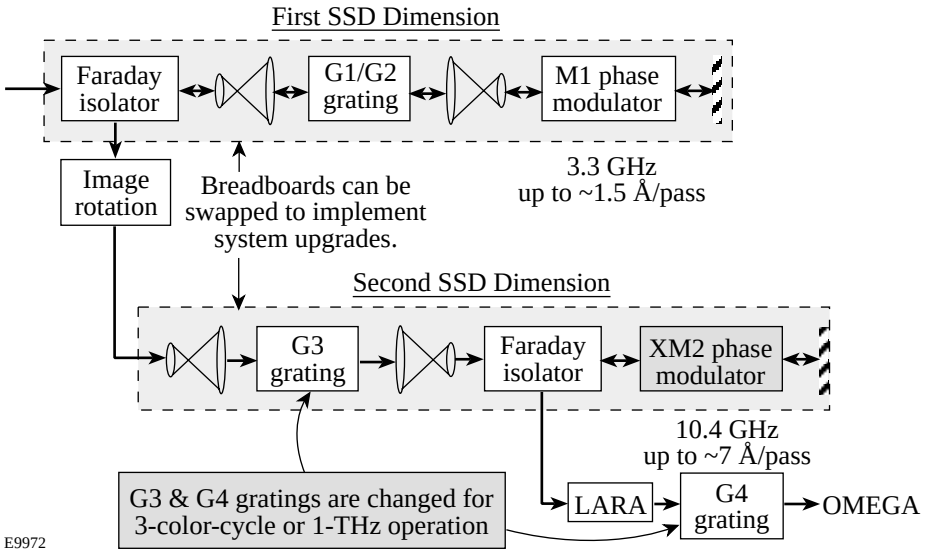

Figure 80.8
A double-pass, 2-D SSD architecture increases phase-modulator efficiency and reduces the space envelope required for a 2-D SSD system.

The two most important aspects of system performance for the improved 2-D SSD systems developed for OMEGA are bandwidth and FM-to-AM conversion. The 2-D SSD system is utilized as a "two-dimensional spectrometer" to measure the SSD bandwidths generated by each modulator, while an infrared streak camera system was developed to identify, measure, and minimize FM-to-AM conversion in the 2-D SSD system, as detailed below.

Accurate SSD bandwidth measurements for both phase modulators can be obtained simultaneously by capturing a far-field image of an SSD beam, as shown in Fig. 80.9, since the bandwidth generated by each phase modulator is dispersed in essentially orthogonal directions. Corrections for inexact dispersion matching between gratings G3 and G4, as well as imprecise image rotation between SSD directions, are accounted for using image-unwarping algorithms. The phase-modulation depth produced by each modulator is then determined by identifying the value for which a simulated spectrum best reproduces the measured spectral lineouts in each SSD direction, including the instrument's point spread function. For the three-color-cycle 2-D SSD system, FM spectra produced by the 10.4-GHz modulator are self-calibrating since the individual FM sidebands are completely resolved and the modulation frequency is accurately known.

Measuring the FM-to-AM conversion performance of the 2-D SSD systems is difficult, particularly for the 10.4-GHz modulation, since an instrument with sufficient bandwidth to measure the microwave modulation frequency and its harmonics is required. Additionally, the ability to verify performance across the beam profile is also important since some FM-to-AM conversion mechanisms manifest themselves in local variations. These requirements, plus the low repetition rate of our SSD pulses (5 Hz), eliminate sampling techniques and make an infrared streak camera the best instrument. The

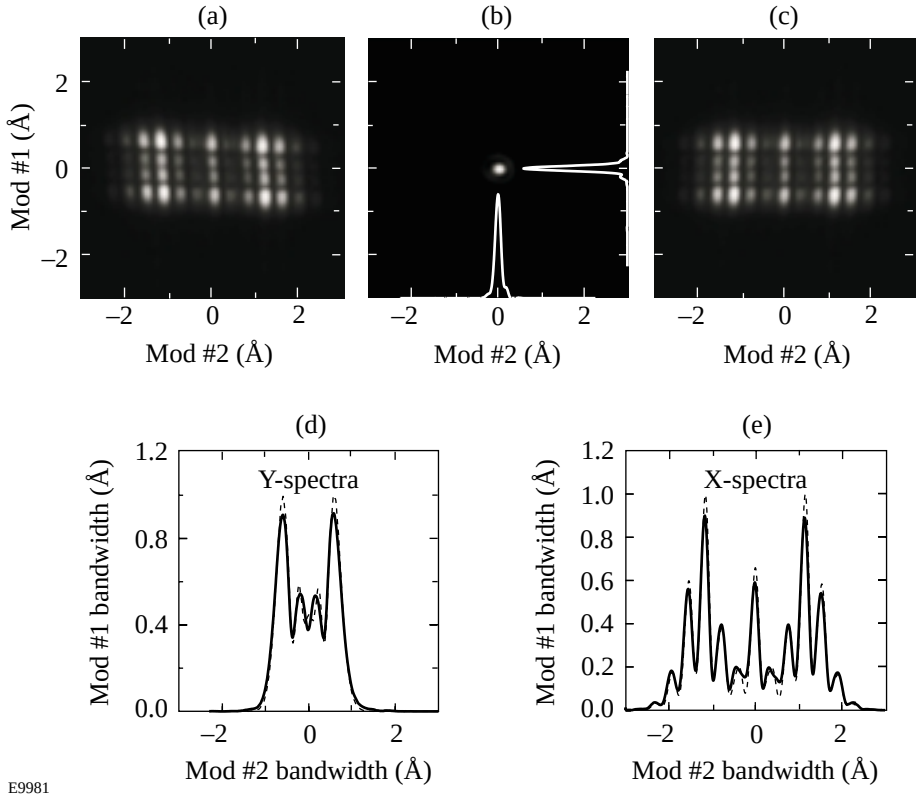

Figure 80.9
Far-field images of the 2-D SSD can be evaluated to measure FM bandwidth produced by each SSD modulator. (a) A raw image is captured on a scientific CCD. (b) The image for an unmodulated pulse is also captured to establish the instrumental response. (c) The image is corrected to account for image rotation errors introduced by the 2-D SSD system. In the corrected image, the bandwidth produced by each modulator is dispersed in orthogonal directions. (d) and (e) The bandwidth produced by each modulator is estimated by finding the simulated spectra (dashed), including the instrumental response, that best fit the measured spectra (solid).

uncoated photocathode of the streak camera is index matched to a wedged, AR-coated window to eliminate spurious etalon effects that would otherwise introduce amplitude modulation artifacts. Streak camera flat-field and time-base corrections are applied to account for instrumental nonlinearities.

FM-to-AM conversion in the 2-D SSD system is discriminated from modulation in the shaped-pulse input by transmitting a reference signal sampled before the 2-D SSD system to the streak camera using an optical fiber, as shown in Fig. 80.10(a). Lineouts at different spatial locations of the streak image [Fig. 80.10(b)] are normalized to this reference signal and the amplitude modulation estimated by finding the peak-to-valley variations of the ratio of these signals [Fig. 80.10(c)]. The signal-to-noise ratio of this measurement depends on the number of pixel rows averaged to produce the lineouts and appears to be limited by photon statistics. The harmonic content of the AM is easily obtained by fast Fourier transforming the difference of the signal and reference lineouts, as shown in Fig. 80.10(d). Statistically analyzing multiple streak images provides estimates of the uncertainty of these measurements.

FM-to-AM conversion in the 2-D SSD system was minimized by adjusting various system parameters and parametrically plotting the measured amplitude modulation to identify the optimal settings. For example, it is well known that propagation from an image plane of an SSD grating results in amplitude modulation. Amplitude modulation is minimized at an image plane of a grating that disperses SSD bandwidth. If an SSD grating is not properly located at the image plane of earlier gratings, the phase relationships between FM sidebands are disturbed and irreversibly convert FM to AM. SSD grating imaging was accomplished by plotting the measured AM as a function of image relay position, as shown in Fig. 80.11(a).

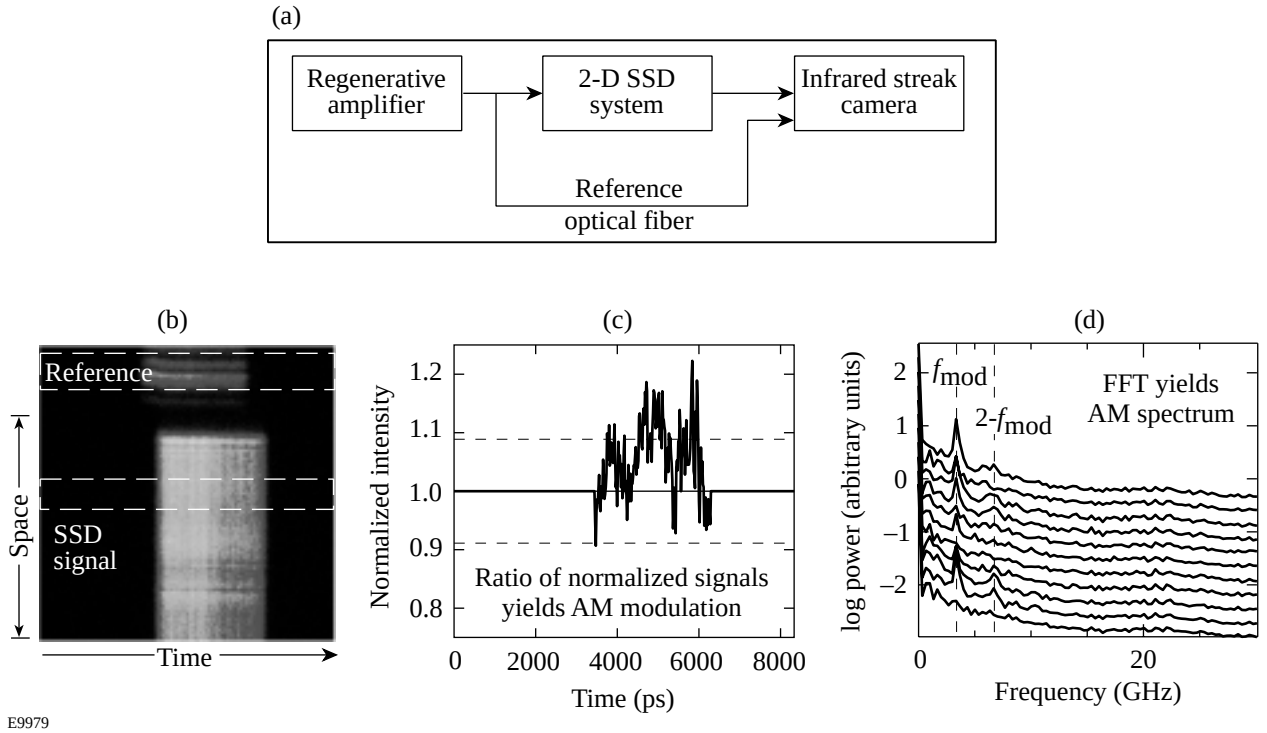

Figure 80.10

An infrared streak camera was employed to identify and measure sources of FM-to-AM conversion. (a) Streak camera measurements of FM-to-AM conversion were performed by comparing the pulse shape at the image plane of the SSD gratings after the SSD system to the pulse shape injected into the 2-D SSD system that is sampled by an optical fiber. (b) The SSD region is divided into regions, and average row lineouts are calculated. A reference pulse shape from the optical fiber delayed input is also acquired. The SSD and reference signals are energy normalized and aligned in time. (c) The ratio of each SSD signal to the reference is used to measure the FM-to-AM conversion. The peak-to-valley in a 333-ps sliding window is calculated for each lineout, and the average value is used as an estimate for the AM. (d) The spectra of the amplitude modulation for a number of different image conditions shown in Fig. 80.11(a) show peaks at the modulation frequency (3.3 GHz) as well as the second harmonic (6.6 GHz) when grating imaging is not optimized. An underlying 1/*f*-like noise spectrum is evident that limits the minimum measurable AM even when no SSD is applied to the beam.

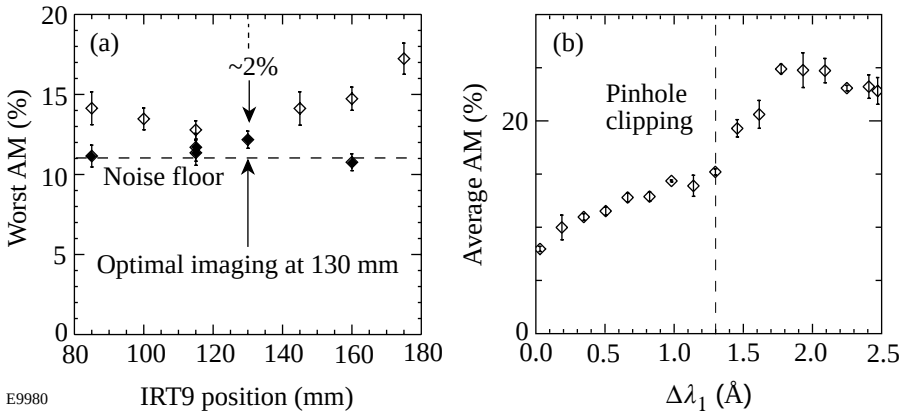

Figure 80.11
AM measurements described in Fig. 80.10 are used to optimize the 2-D SSD system performance. (a) SSD grating imaging is set by minimizing amplitude modulation. Measured AM grows linearly as a function of image plane separation, except near the noise floor where it adds in quadrature with the noise. (b) The onset of pinhole clipping in the slotted LARA spatial filter (1.0×1.8 mm) is characterized by scanning bandwidth produced by the first modulator. The final slotted pinhole dimensions (1.0×2.4 mm) were set to accommodate the specified 1.5 Å, plus extra margin for operational tolerances.

The length of the major axis of the slotted LARA spatial-filter pinhole was also established using this method, as shown in Fig. 80.11(b). The bandwidth generated by the first SSD modulator is dispersed before the LARA. As bandwidth is increased for a given pinhole size, pinhole clipping causes the measured AM values to increase rapidly. For a 1.0×1.8-mm pinhole, clipping is first observed at a bandwidth of approximately 1.3 Å. The final slotted pinhole (1.0×2.4 mm) should maximize spatial-filtering effects while maintaining reasonable operational tolerances.

Summary

Direct-drive ICF experiments require a laser system with excellent irradiation uniformity. Major elements of LLE's beam-uniformity program have been completed, including demonstration of a 10.4-Ghz bulk-phase modulator capable of producing either large SSD bandwidths or multiple color cycles, implementation of a flexible double-pass 2-D SSD architecture, and diagnostics for quantifying the performance of these improved smoothing techniques. The remaining elements of this program will be completed when broadband (1-THz) 2-D SSD is implemented on OMEGA later this year.

ACKNOWLEDGMENT

This work was supported by the U.S. Department of Energy Office of Inertial Confinement Fusion under Cooperative Agreement No. DE-FC03-92SF19460, the University of Rochester, and the New York State Energy Research and Development Authority. The support of DOE does not constitute an endorsement by DOE of the views expressed in this article.

REFERENCES

1. S. Skupsky and R. S. Craxton, Phys. Plasmas **6**, 2157 (1999).
2. S. Skupsky, R. W. Short, T. Kessler, R. S. Craxton, S. Letzring, and J. M. Soures, J. Appl. Phys. **66**, 3456 (1989).
3. A. Babushkin, J. H. Kelly, C. T. Cotton, M. A. Labuzeta, M. O. Miller, T. A. Safford, R. G. Roides, W. Seka, I. Will, M. D. Tracy, and D. L. Brown, in *Third International Conference on Solid State Lasers for Application to Inertial Confinement Fusion*, edited by W. H. Lowdermilk (SPIE, Bellingham, WA, 1999), Vol. 3492, pp. 939–943.
4. J. M. Auerbach *et al.*, Appl. Opt. **18**, 2495 (1979).
5. I. F. Stowers and H. G. Patton, in *Laser-Induced Damage in Optical Materials: 1977*, edited by A. J. Glass and A. H. Guenther, Natl. Bur. Stand. (U.S.), Spec. Publ. 509 (U.S. Government Printing Office, Washington, DC, 1977), pp. 440–454.
6. W. W. Simmons and W. E. Warren, *Laser Program Annual Report 1978*, Lawrence Livermore National Laboratory, Livermore, CA, UCRL-50021-78, **2**, 7-111 (1978).
7. D. C. Brown, in *High-Peak-Power Nd:Glass Laser Systems*, edited by D. L. MacAdam, Springer Series in Optical Sciences (Springer-Verlag, Berlin, 1981), Chap. 7.
8. J. E. Murray *et al.*, in *Solid-State Lasers for Application to Inertial Confinement Fusion (ICF)*, edited by W. F. Krupke (SPIE, Bellingham, WA, 1995), Vol. 2633, pp. 608–614.